Spatially adaptive grand canonical ensemble Monte Carlo simulations

A. Chatterjee,[1] M. A. Katsoulakis,[2] and D. G. Vlachos[1,*]
[1]*Department of Chemical Engineering and Center for Catalytic Science and Technology, University of Delaware, Newark, Delaware 19716-3110, USA*
[2]*Department of Mathematics and Statistics, University of Massachusetts, Amherst, Massachusetts 01003-3110, USA*
(Received 23 March 2004; published 9 February 2005)

A spatially adaptive Monte Carlo method is introduced directly from the underlying microscopic mechanisms, which satisfies detailed balance, gives the correct noise, and describes accurately dynamic and equilibrium states for adsorption-desorption (grand canonical ensemble) processes. It enables simulations of large scales while capturing sharp gradients with molecular resolution at significantly reduced computational cost. *A posteriori* estimates, in the sense used in finite-elements methods, are developed for assessing errors (information loss) in coarse-graining and guiding mesh generation.

DOI: 10.1103/PhysRevE.71.026702 PACS number(s): 02.70.Ns, 02.70.Tt, 61.46.+w, 82.20.Wt

INTRODUCTION

Monte Carlo (MC) is one of the most widespread molecular simulation tools in science and engineering [1,2]. MC applications range from the modern areas of biotechnology and nanotechnology to catalysis to crystal growth to image processing to stochastic optimization. Due to its discrete nature of moving one atom at a time, MC is computationally very intensive. As a result, MC is typically limited to bulk-like systems (studied via periodic boundary conditions) or nanoscale systems. On the other hand, many systems are significantly larger (e.g., microporous membranes and nanotubes of many micrometers in length) and features in many experimental systems, such as in catalytic reactions on single crystals and in image processing, are often several microns in size (see for example [3]). It is clear that multiscale modeling and simulation are needed to enable study of phenomena over scales beyond the realm of currently available molecular models.

Different multiscale tools, reviewed in [4], offer the possibility of extending MC simulations to larger scales. One class is the *onion-type* hybrid MC-deterministic multiscale models that are based on domain decomposition with overlapping subdomains. Here MC is applied only in a small part of the simulation domain, where microscopic phenomena are important, and a deterministic model is employed in the rest of the domain, where the continuum approximation is valid. This has been the most advanced type of multiscale simulation [5–15]. In systems where there is no separation of length scales and associated phenomena, the hybrid *multigrid-type* or gap-tooth method can be employed [16–18]. Here a physical domain is partitioned in coarse cells where conservations laws are advanced by a deterministic simulator. Within each coarse cell (or at interfaces) microscopic simulators are applied to compute fine scale information that is passed to the coarse level simulator. The coarse level simulator in turn passes information so microscopic simulators are appropriately constrained. Despite significant advances in hybrid multiscale simulations, they have certain shortcomings. These include numerical instabilities and a difficulty in ensuring conservation across interfaces (see [4] for specific examples). Furthermore, noise is adversely affected, which in turn alters fluctuations-driven physical phenomena [14]. There is therefore a need to develop alternative strategies that overcome these problems.

The coarse-grained MC (CGMC) simulation introduced recently in [19–21] attempts to overcome these problems. CGMC groups microscopic lattice points into uniformly sized coarse cells and coarse grains, directly from the microscopics, energetics and transition probabilities to obey detailed balance and continuum constitutive equations. It has been found that CGMC preserves the noise, does not exhibit numerical instabilities, and gives significant computational savings. However, most problems, whose solution is spatially nonuniform, exhibit a separation of length scales, such as an internal boundary layer or an interface where large gradients exist only in a relatively small, *high activity* regime that is adjacent to a large, *low activity* regime of low gradients. As an example, traveling waves arising in catalytic reactions [3] and during the epitaxial growth of materials (emanating from a growing cluster on a substrate)[22] exhibit precisely such a separation of length scales. Large gradients in high activity regimes demand microscopic resolution. As a result, a CGMC with a uniform cell size will be almost equally demanding with a conventional MC simulation. Therefore, it is important to introduce a multiresolution framework of dynamic CGMC simulation that is capable of having atomistic scale resolution in high activity regimes and coarse resolution in low activity regimes. Furthermore, it is important to develop mathematical evaluation criteria for carrying out such model refinement procedures in moving from coarser to finer MC methods and vice versa.

In this paper we introduce such a framework and demonstrate its feasibility with illustrative examples in the grand canonical ensemble. A critical point in our development is that the new framework obeys, by design, detailed balance and gives the proper noise. The last point is imperative to correctly simulating noise-controlled phenomena such as nucleation, nonlinear dynamics, pattern formation and selection, and image processing. This is a major advantage of our

*Corresponding author.

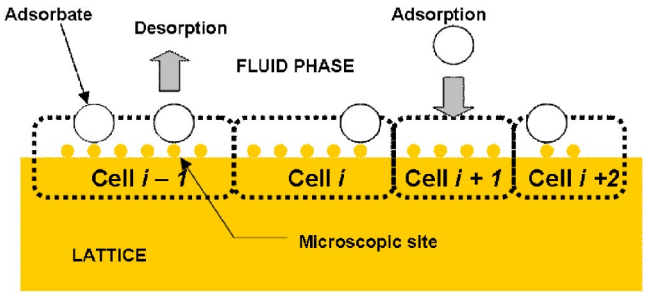

FIG. 1. (Color online) Schematic of a nonuniform lattice for exchange of atoms between a coarse cell and the fluid phase.

approach compared to other hybrid multiscale models mentioned above. Furthermore, we propose error estimates to assess the loss of information during coarse-graining, which depends only on the CGMC observables [see Eq. (12) below]. These are *a posteriori* estimates in the terminology of the finite element literature [23], and thus can be used to assess on-the-fly the numerical error (since they depend only on the CGMC) and design the level of coarse-graining accordingly.

MICROSCOPIC PROCESSES AND SPATIALLY ADAPTIVE, COARSE-GRAINED PROCESSES

The prototype system studied here involves adsorption and desorption processes of interacting particles on a microscopic lattice $\mathcal{L}$ of N sites. Physically, this system is a fundamental building block of adsorption on single crystals and microporous materials and of surface reactions and crystal growth models. In analogy with the Ising model, a microscopic site at location $z \in \mathcal{L}$ is characterized by an order parameter, $\sigma(z)$, which is either $\sigma(z)=1$ (an occupied site) or $\sigma(z)=0$ (an unoccupied site). In the Ising model terminology, adsorption and desorption correspond to a spin flip mechanism.

The energy of the system is given by the Hamiltonian

$$H(\underline{\sigma}) = -\frac{1}{2}\sum_{z\in\mathcal{L}} U(z)\sigma(z)$$

$$= -\frac{1}{2}\sum_{y\in\mathcal{L}}\sum_{z\neq y} J(|y-z|)\sigma(y)\sigma(z) + \sum_{z\in\mathcal{L}} h\sigma(z), \quad (1)$$

where $\underline{\sigma}$ is a vector containing the spin configurations of the entire lattice $\mathcal{L}$, h is the external field, such as the chemical potential, and J is the potential of adsorbate-adsorbate interactions. The interaction energy of an adsorbate at site z with adsorbates on the rest of the lattice is denoted as $U(z) = \Sigma_{y\in\mathcal{L}} J(|y-z|)\sigma(y) - h$.

In the proposed adaptive CGMC method, a coarse lattice $\mathcal{L}_c$ is defined by grouping neighboring microcells into m coarse cells of variable size (see Fig. 1). Each coarse cell D_k $(k \in 1,\ldots,m)$ consists of q_k microcells. We define the projection operator F from microscopic to coarse variables, so that the coarse-grained order parameter (still an integer)

$$F(\sigma)(k) = \eta_k = \sum_{y\in D_k} \sigma(y), \quad k = 1,\ldots,m \quad (2)$$

at D_k satisfies the constraint $0 \leqslant \eta_k \leqslant q_k$. The fractional value of the order parameter, $\overline{\eta}_k = q_k^{-1}\eta_k$, is denoted as the coverage.

In large-scale systems and especially in regimes of low activity, the order parameter does not vary considerably within a coarse cell. As a result, local mean field is assumed within each coarse cell yielding a closure at the stochastic level. The coarse-grained Hamiltonian of the system is derived from Eq. (1) and is

$$\overline{H}(\underline{\eta}) = -\frac{1}{2}\sum_{k\in\mathcal{L}_c} \overline{U}_k\eta_k$$

$$= -\frac{1}{2}\sum_{k\in\mathcal{L}_c}\sum_{l\in\mathcal{L}_c, l\neq k} \overline{J}_{kl}\eta_k\eta_l - \frac{1}{2}\sum_{k\in\mathcal{L}_c} \overline{J}_{kk}\eta_k(\eta_k-1)$$

$$+ \sum_{k\in\mathcal{L}_c} h\eta_k, \quad (3)$$

where $\underline{\eta}$ is the configuration space (vector containing the coarse-grained order parameters for the lattice) and $\overline{J}_{kl}$ is the energy of interaction of an adsorbate in coarse cell k with all adsorbates present in coarse cell l. The energy of interaction of an adsorbate in kth coarse cell, $\overline{U}_k$, with adsorbates on the rest of the lattice is

$$\overline{U}_k = \overline{U}(z) = \overline{J}_{kk}(\eta_k - 1) + \sum_{l\in\mathcal{L}_c, l\neq k} \overline{J}_{kl}\eta_l - h. \quad (4)$$

The summation extends over all interacting cells whose number depends on the length of the potential L and the coarse-grained mesh. By splitting $\overline{U}_k$ and the Hamiltonian into interactions within a coarse cell and interactions with neighboring cells, both the microscopic MC and global mean field models are recovered in the corresponding limit.

The transition probabilities on the microscopic lattice for adsorption and desorption are, respectively,

$$c_a(z,\underline{\sigma}) = k_a P(1-\sigma(z)) \quad (5)$$

and

$$c_d(z,\underline{\sigma}) = k_d e^{-\beta U(z)}\sigma(z), \quad (6)$$

where k_a and k_d are the adsorption and desorption rate constants, $\beta=(k_B T)^{-1}$ is the inverse temperature (k_B is the Boltzmann constant and T is the absolute temperature), and P is the partial pressure of adsorbing species. The coarse-grained transition probabilities are derived as outlined in [19] and are

$$c_a(k,\underline{\eta}) = k_a P(q_k - \eta_k) = d_0(q_k - \eta_k)e^{-\beta h} \quad (7)$$

for adsorption and

$$c_d(k,\underline{\eta}) = k_d\eta_k e^{-\beta\overline{U}_k} = d_0\eta_k e^{-\beta(\overline{U}_k + U_0)} \quad (8)$$

for desorption. These are intuitively obvious. On the other hand, the nonintuitive term $\eta_k(\eta_k-1)$ in Eq. (3) represents the contribution to the Hamiltonian from the interactions within a coarse cell. In previous work, this term has been incorrectly postulated [24] leading to violation of detailed

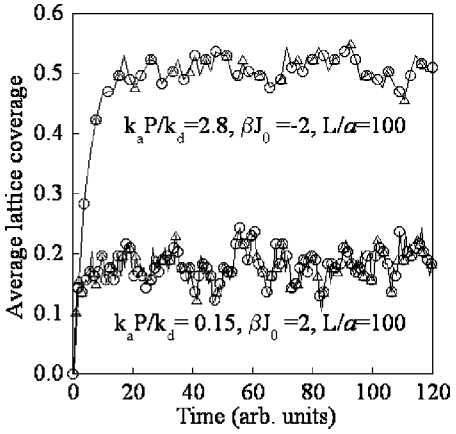

FIG. 2. Uptake for two sets of parameters using different coarse meshes, $\omega=1$ (solid line, microscopic lattice), 1.05 (circles), and 1.2 (triangles). For $\beta J_0=-2$, the time is multiplied by a factor of 30. The total number of microscopic cells is $N=300$.

balance, at least for adsorption-desorption processes. The latter could lead to significant errors in solutions under certain conditions [19,20]. The same applies to the term (η_k-1) in $\overline{U_k}$. Finally, the interaction terms $\overline{J_{kl}}$ are computed by projecting the microscopic potential on a Haar wavelet basis as discussed in [20].

An essential feature of a correct adaptive mesh is to ensure that the transition probabilities obey detailed balance. Upon an adsorption-desorption event at D_k, the order parameter vector $\underline{\eta}$ is modified by the unit vector $\underline{\delta}_k$, and it is required that

$$\mu(\underline{\eta})c_a(k,\underline{\eta}) = \mu(\underline{\eta}+\underline{\delta}_k)c_d(k,\underline{\eta}+\underline{\delta}_k), \tag{9}$$

$$\mu(\underline{\eta})c_d(k,\underline{\eta}) = \mu(\underline{\eta}-\underline{\delta}_k)c_a(k,\underline{\eta}-\underline{\delta}_k). \tag{10}$$

The limiting distribution of the configuration space $\mu(\underline{\eta})$ gives the probability of the system existing in state $\underline{\eta}$. Following the procedure of [19], it is straightforward to show that detailed balance is satisfied for adaptive meshes introduced here.

MONTE CARLO SIMULATIONS OF ADAPTIVE COARSE-GRAINED PROCESSES

Next we present illustrative examples in one and two dimensions (1D and 2D) to illustrate the feasibility of the adaptive CGMC method and evaluate the savings in CPU. First, we examine the correctness of the dynamics, equilibrium states, and the noise in the presence of interactions. This is a prototype statistical mechanics problem (for first nearest-neighbor interactions, see [25]). Figure 2 shows the uptake on an initially empty 1D lattice where the adaptive cells are set arbitrarily in a geometric sequence starting from a microscopic cell on the left and increasing the cell size by ω from its previous one, i.e., $q_{k+1}=\omega q_k$ (note that each q_k is truncated into an integer number and the last cell accommodates the remaining microscopic cells so that the total number N of simulated microscopic cells is fixed). A piecewise constant, long-ranged potential is used in all simulations. Results are shown for attractive interactions–low pressure (lower set of data) and repulsive interactions–high pressure (upper set of data). It is found that the adaptive mesh CGMC captures the correct transient behavior and equilibrium states. Furthermore, the noise of adaptive CGMC is nearly identical to that of the microscopic MC over the entire domain, yielding pathwise agreement between the two. This pathwise agreement stems in part from the fact that the potential is sufficiently long-ranged, so the local mean field assumption is an excellent closure approximation, and in part from the fact that the same sequence of random numbers are used at each event for microscopic MC and adaptive CGMC. CGMC gives very good results even for short-ranged potentials (see examples in [19–21]).

In the above example, there is no real need for an adaptive mesh. Next we present two problems where adaptive MC is essential. The first addresses the calculation of standing waves in 1D. In the case of strongly attractive long-range interactions, the global mean field isotherm $[k_aP(1-\theta)=k_de^{-\beta J_0\theta_\theta}]$ is multivalued, and at equilibrium, a dense and a dilute phase coexist [the coexistence line is given by $k_aP/k_d=\exp(-\beta J_0/2)$]. For a piecewise constant, long range potential, an analytical solution describing the standing wave connecting the two coexisting phases exists:

$$\theta(x) = \frac{1}{2}[(2\theta_+ - 1)\tanh(\beta J_0(2\theta_+ - 1)x) + 1]. \tag{11}$$

Here θ_+ is the equilibrium coverage of the dense phase (solution of the global mean field isotherm) and $\beta J_0=\beta\Sigma_{-L\leqslant y\leqslant L}J(|y-z|)$ is the zeroth moment of the potential.

This is an excellent benchmark problem of adaptive mesh CGMC because the interface separating the two phases is of microscopic size at low temperatures whereas the domain of each phase is semi-infinite. Adsorption and desorption simulations in the grand canonical ensemble are carried out by initially portioning the lattice into two equal size parts, one with a coverage θ_+ and the other with θ_- (θ_+ and θ_- are the equilibrium coverages of the dense and dilute phases, respectively; θ_+ and θ_- are obtained using two independent MC simulations with periodic boundary conditions and a uniform initial coverage over the entire domain). Using periodic boundary conditions, two standing waves are formed located roughly at $x=0$ and 0.5 (the dimensionless distance is defined as $x=X/Na$, where X is the distance of the center of the coarse cell from one edge of the lattice and a is the microscopic lattice size). The squares in Fig. 3(a) show the excellent agreement of a uniform mesh of $q=64$ with the analytical solution given by the solid line but highlight that the standing wave is barely resolved.

Information theory is used in order to assess the error in adaptive CGMC methods following ideas introduced in [21]. By defining the maximum difference in interaction between two cells, $j_{kl}=\max|J(x-y)-J(x'-y')|, x,x'\in D_k, y,y'\in D_l$, an upper bound for the relative entropy (loss of information), $\int \log(d\mu_{m,q,\beta}/d\mu_{\mathcal{L},\beta^0F})d\mu_{m,q,\beta}$, between the microscopic and the adaptive CGMC can be computed

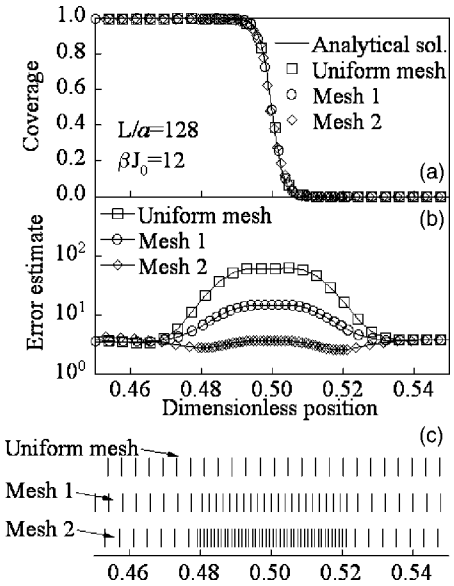

FIG. 3. (a) Comparison of steady state analytical standing wave solution to adaptive CGMC simulation for parameters indicated. (b) Error estimates in coverage using a uniform mesh ($q=64$, $m=256$, squares) and two adaptive meshes (circles and diamonds). (c) Meshes around the interface. The total number of microscopic cells is $N=16384$.

$$\varepsilon_k = 4\sum_k \frac{j_{kk}}{q_k(q_k-1)}\langle \eta_k(q-\eta_k)[\eta_k(\eta_k-1)+(q-\eta_k) \times (q-\eta_k+1)]\rangle + 4\sum_k \sum_{l\neq k} \frac{j_{kl}}{q_k q_l}\langle q^2\eta_l(q-\eta_l) - 2\eta_k\eta_l \times (q-\eta_k)(q-\eta_l)\rangle, \quad (12)$$

where the brackets denote ensemble average, $\mu_{m,q,\beta}$ is the coarse-grained Gibbs measure, and $\mu_{\mathcal{L},\beta^0}F$ is the coarse-graining of the microscopic Gibbs measure. Simulations have confirmed that the scaling laws of error in coarse-graining can adequately be described using Eq. (12).

Relation (12) allows one to design adaptively the coarse MC simulation with a desired accuracy. Inspection of the theoretical error estimate reveals that this term penalizes interfaces in transitions from a high to a low coverage area and vice versa. As a result, an adaptive method has finer grid points on the transition region rather than on the two phases themselves. We remark here the notable similarity to the finite element literature for viscous hyperbolic equations, where regions of (viscous) shock waves are resolved to a greater extent than smooth regions by employing *a posteriori* estimates; see for instance [26].

The squares in Fig. 3(b) show the error estimate obtained using Eq. (12) for the uniform mesh with $q=64$. Coverages and error estimates in each cell are expected values from time intervals of 10^6 MC events each per simulation as well as 20 independent MC simulations. As expected, the error is maximum at the interface. Commonly used strategies for adaptive mesh refinement, such as the equidistribution of error or node insertion, can be implemented for reducing the error in the solution. Here a simplified version of the latter is employed. In particular, cells with an error estimate greater than a threshold (taken to be 5.0 in Fig. 3) are divided into two smaller cells of equal size. The coarse-grained order parameter is also divided equally between the two new cells. In the event when either the cell size or the occupancy is an odd integer, one of the cells and/or one of the order parameters are made larger by 1. The adaptive mesh (denoted as mesh 1 in Fig. 3) generated this way is shown in Fig. 3(c). It consists of smaller cells of uniform size q_1 around the interface (in the range $0.48<x<0.52$) and larger cells of uniform size $q_2=64$ elsewhere. A second mesh refinement is performed based on the solution obtained on mesh 1 to get a finer mesh around the interface. This mesh 2 is also depicted in Fig. 3(c).

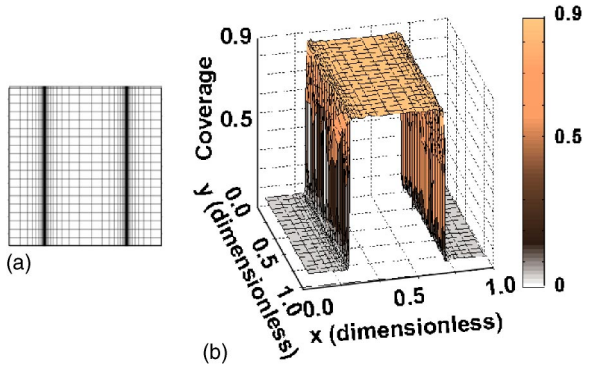

FIG. 4. (Color online) (a) Adaptive mesh used. (b) 2D steady state coverage profile. The pressure is discontinuous at the indicated locations. Total number of microscopic cells are $N_x=10544$ and $N_y=300$ along the x and y axis, respectively.

The adaptive MC results (circles and diamonds) are in excellent agreement with the analytical solution and resolve the interface much more accurately as judged from the number of cells placed at the interface and the reduction in error (the CPU of the finest mesh is approximately larger by a factor of 2 but the maximum error is approximately 16 times smaller). Thus, *a posteriori* error estimates offer a judicious way of designing meshes of adaptive CGMC for stochastic simulation. More efficient strategies for mesh refinement will be subject of future work.

Last we present a second example in 2D where the pressure field is nonuniform. External field nonuniformity arises in many practical systems, such as deposition from high pressure gases, catalytic reactors, etc. as well as variations of the surface temperature. In the presence of phase transitions on the surface, very abrupt (nearly discontinuous) changes in the external field are expected for coupled surface-fluid problems. Macroscopically, these abrupt changes in the external field are demonstrated as ignitions and extinctions. In our example, a square pressure pattern in the x direction and periodic in the y direction is used. The microscopic lattice consists of 300 cells in the y direction by 10^5 cells in the x direction. This lattice choice corresponds to actual lengths of $0.3\ \mu\text{m}\times 100\ \mu\text{m}$ (assuming a lattice spacing of ~ 1 nm). The adaptive mesh is depicted in Fig. 4(a) with fine mesh near the discontinuities of pressure and coarse mesh at re-

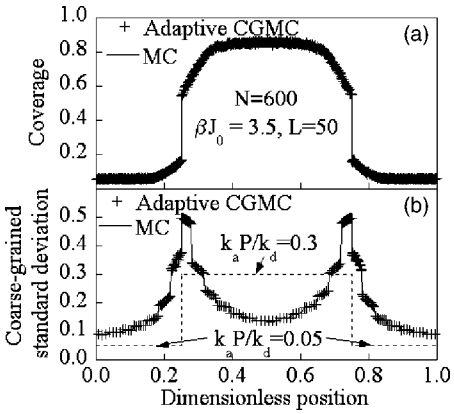

FIG. 5. Comparison of (a) steady state coverage profile and (b) the corresponding noise in coverage from microscopic MC and adaptive CGMC. The noise is comparable over the same length scale, e.g., in microscopic regimes. The adaptive mesh is indicated by the spacing between points. The total number of microscopic cells is $N=600$; the other parameters are those of Fig. 4.

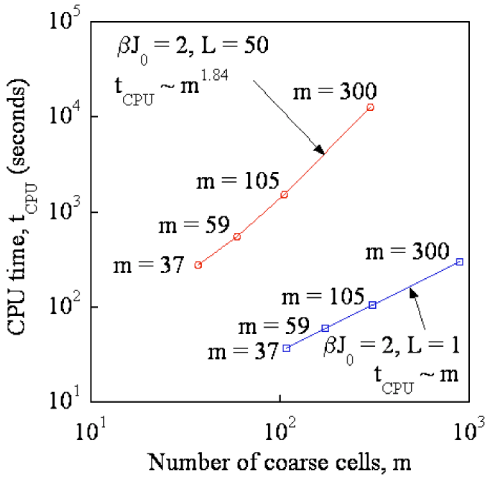

FIG. 6. (Color online) CPU vs number of coarse cells in adaptive mesh MC for two potential lengths indicated. The parameters are $\beta J_0=2$, $N=300$, $k_aP=1$, and $k_d=1$. The values of ω corresponding to the depicted values of m are 1, 1.02, 1.05, and 1.1.

mote regions. Figure 4(b) shows the time average coverage and the pressure field is depicted in Fig. 5(b). The CPU is 6 minutes for performing this simulation on a Pentium 4 2.4 GHz processor. It is estimated that it will require about 1892 years to do this simulation with a microscopic KMC.

Figure 5(a) shows the expected value of the coverage vs position for the conditions of 2D simulations of Fig. 4 but for a small, 1D domain where microscopic MC with good statistics is still feasible. Figure 5(b) compares the corresponding microscopic and coarse MC noise at steady state and also depicts the discontinuous pressure profile. Note that the noise in the microscopic MC is obtained over the same length scales as the adaptive CGMC and is given by

$$s_k = \sqrt{\left\langle \left(\frac{1}{q_k} \sum_{y \in D_k} \sigma(y) \right)^2 \right\rangle - \left\langle \frac{1}{q_k} \sum_{y \in D_k} \sigma(y) \right\rangle^2}. \quad (13)$$

Figure 5(b) indicates that the noise of adaptive CGMC is practically identical to the microscopic MC in regions of high resolution. This is an important point indicating that adaptive CGMC can correctly capture the noise at sharp interfaces and in noise controlled phenomena, such as nucleation and growth, which are localized at a moving interface. The adaptive CGMC can correctly capture not just the overall noise (Fig. 2) but also spatially resolved noise [Fig. 5(b)].

Finally, we have performed a number of 1D simulations under a uniform pressure field for short and long potentials to assess the savings in CPU. Simulations have been conducted for a total of 6×10^6 MC events, which correspond to approximately the same real time as the mesh coarsens. The lattice starts with a microscopic cell at one end and varies from one cell to the next using a geometric sequence. The CPU results are depicted in Fig. 6. For short potentials where the number of operations in computing energies is small, the CPU is reduced linearly with decreasing number of coarse cells. On the other hand, for long-range interactions, e.g., $L/a=50$, where several operations are needed to compute the cell interaction energies, the CPU reduces almost quadraticly (CPU $\sim m^{1.8}$). Obviously, details of the exponent would depend on the specifics of the mesh. Additional q^2 savings are expected for canonical ensemble (diffusion) simulations. It is clear that significant savings can result using the proposed adaptive mesh CGMC method.

CONCLUSIONS

In summary, we have introduced a new multiresolution framework for performing dynamic Monte Carlo (MC) simulation. This method is essential for systems of mesoscopic length scales and when interfaces, boundary conditions, internal boundary layers demand a microscopic resolution in some high activity (large gradients) regimes but are tolerable to coarse graining in other, low activity (low gradients) regimes. The proposed framework obeys detailed balance, gives asymptotically the same noise as the microscopic MC at the same length scale, and the correct dynamics and equilibrium states. The correct noise sets our method apart from other multiscale methods and makes it the only suitable one for noise-controlled phenomena. The substantial computational savings enable multiresolution MC simulation of complex systems with separation in length scales. Information loss theory provides *a posteriori* estimates of the errors for this new framework that can be used to guide the mesh development. The new method could enable simulations over large scales in numerous applications ranging from nucleation and growth to nonlinear dynamics to pattern formation and selection to image processing.

ACKNOWLEDGMENTS

This research was partially supported by NSF through ITR-0219211, DMS-0100872, and CTS-0312117.

[1] K. Binder, *Monte Carlo Methods in Statistical Physics* (Springer-Verlag, Berlin, 1986), Vol. 7.
[2] D. P. Landau and K. Binder, *A Guide to Monte Carlo Simulations in Statistical Physics* (Cambridge University Press, Cambridge, England, 2000).
[3] G. Ertl, Science **254**, 1750 (1991).
[4] D. G. Vlachos Adv. Chem. Eng. (to be published).
[5] T. P. Schulze, P. Smereka, and E. Weinan, J. Comput. Phys. **189**, 197 (2003).
[6] S. Raimondeau and D. G. Vlachos, Chem. Eng. J. **90**, 3 (2002).
[7] D. G. Vlachos, AIChE J. **43**, 3031 (1997).
[8] R. Alkire and M. Verhoff, Electrochim. Acta **43**, 2733 (1998).
[9] P. D. Christofides, AIChE J. **47**, 514 (2001).
[10] R. Lam and D. G. Vlachos, Phys. Rev. B **64**, 035401 (2001).
[11] T. J. Pricer, M. J. Kushner, and R. C. Alkire, J. Electrochem. Soc. **149**, C396 (2002).
[12] T. J. Pricer, M. J. Kushner, and R. C. Alkire, J. Electrochem. Soc. **149**, C406 (2002).
[13] T. O. Drews, J. C. Ganley, and R. C. Alkire, J. Electrochem. Soc. **150**, C325 (2003).
[14] T. P. Schulze, J. Cryst. Growth **263**, 605 (2004).
[15] D. G. Vlachos, L. D. Schmidt, and R. Aris, J. Chem. Phys. **93**, 8306 (1990).
[16] M. Tammaro, M. Sabella, and J. W. Evans, J. Chem. Phys. **103**, 10277 (1995).
[17] C. W. Gear, J. Li, and I. G. Kevrekidis, Phys. Lett. A **316**, 190 (2003).
[18] E. Weinan, B. Engquist, and Z. Y. Huang, Phys. Rev. B **67**, 092101 (2003).
[19] M. Katsoulakis, A. J. Majda, and D. G. Vlachos, Proc. Natl. Acad. Sci. U.S.A. **100**, 782 (2003).
[20] M. A. Katsoulakis, A. J. Majda, and D. G. Vlachos, J. Comput. Phys. **186**, 250 (2003).
[21] M. A. Katsoulakis and D. G. Vlachos, J. Chem. Phys. **119**, 9412 (2003).
[22] W. K. Burton, N. Cabrera, and F. C. Frank, Proc. R. Soc. London, Ser. A **243**, 299 (1951).
[23] M. Bieterman and I. Babuska, Numer. Math. **40**, 373 (1982).
[24] A. Ishikawa and T. Ogawa, Phys. Rev. E **65**, 026131 (2002).
[25] T. L. Hill, *An Introduction to Statistical Thermodynamics* (Dover, New York, 1986).
[26] C. Johnson and A. Szepessy, Commun. Pure Appl. Math. **48**, 199 (1995).